

Mechanics Research Communications. 2019	Publication Office: Elsevier UK
Editor-in-Chief: A. Rosato New Jersey Institute of Technology, Newark, New Jersey, USA Anthony.Rosato@njit.edu	ZHANG, G., and CHANSON, H. (2019). "On Void Fraction and Flow Fragmentation in Two-Phase Gas-Liquid Free-Surface Flows." <i>Mechanics Research Communications</i> , Vol. 96, pp. 24-28 & Digital Appendix pp. S1-S6 (DOI: 10.1016/j.mechrescom.2019.01.001) (ISSN 0093-6413).

On Void Fraction and Flow Fragmentation in Two-Phase Gas-Liquid Free-Surface Flows

Gangfu Zhang ^(1,2) and Hubert Chanson ⁽¹⁾ *

¹The University of Queensland, School of Civil Engineering, Brisbane QLD 4072, Australia

²Presently: WSP Pty Limited, Brisbane, QLD 4000, Australia

*Corresponding author h.chanson@uq.edu.au

Tel.: +61-7-3365 4163; fax: +61-7-33654599

Accepted:

Abstract

In free-surface flows, the interactions between high-velocity liquid and atmosphere may lead to strong gas-liquid mixing and complex multiphase flow interactions. In this study, the void fraction power spectrum density (PSD) is used to provide an alternative view of the air-water flow composition. The high frequency range of the PSD curve reflects contributions of small chord times, while the low frequency range contains contributions of both small and large chord times. Likewise, the interactions between the smallest bubbles contribute approximately uniformly to the entire frequency range of the spectrum, while any interaction involving large bubbles/drops will be modulated by $1/f^2$. It is shown that the void fraction spectra are a powerful tool in providing an alternative view of the air-water flow composition.

Keywords: Multiphase flows; Void fraction power spectrum density; Bubble frequency; Free-surface flows..

1. Introduction

The interactions between high-velocity liquids and the atmosphere may lead to strong gas-liquid mixing and complex multiphase flow interactions (Rao and Kobus 1971, Chanson 1997, Crowe et al. 1998). Relevant applications encompass chemical, nuclear, civil, mechanical and environmental engineering situations. The resulting gas-liquid mixture consists of both gas bubbles surrounded by liquid and droplets surrounded by gas, inclusive of foam, spray and complex gas-liquid structures (Hoyt and Taylor 1977, Wood 1991, Felder and Chanson 2016). The entrainment of gas packets can be localised, as at the impingement of plunging jets (Ervin et al. 1980, Bertola et al. 2018), or continuous along the gas-liquid interface, e.g. on a spillway chute (Cain and Wood 1981, Zhang and Chanson 2017) (Fig. 1).

In high-velocity free-surface flows, the gas volume fraction ranges from very small values to unity in the atmosphere. Traditional monophasic flow measurement techniques are affected by the dilute phase and the gas-liquid interfaces. The most robust method is the phase-detection needle probe (Jones and Delhaye 1976, Cartellier and Achard 1991, Chanson 2002, 2016). The probe tip is designed to pierce the

gas-liquid interfaces and the resulting signal is a pseudo-square-wave signal, as illustrated in Figure 2A. Figure 2A shows instantaneous void fraction data (blue curve) and post-processed signal using a single threshold technique. In Figure 2A, each signal drop corresponds to a liquid-to-gas interface, while the following signal rise is a gas-to-liquid interface detection. Over the sampling period, the signal averaging gives the time-averaged void fraction and the rate of liquid-to-gas interface detections yields the bubble frequency.

In the present study, the processing of phase-detection probe signal is re-visited. It is shown that the instantaneous signal of a single-sensor probe includes information in terms of both phase bulk and gas-liquid composition. These properties are developed, and physical observations are discussed.

2. Basic considerations on gas-liquid structure

Considering a streamtube through a phase-detection needle sensor, the flow may be reduced to a streamwise distribution of small discrete gas and liquid elements, comprised of the smallest discrete air-water particles of length scale λ_{aw} , as shown in Figure 2B. λ_{aw} is selected such that the probability of

one element being gas or liquid becomes independent of the adjacent elements. Focusing on each pair of adjacent gas-liquid elements defined as 1 and 2 respectively, a gas-liquid interface is detected when element 1 is gas and element 2 is liquid, or element 1 is liquid and element 2 is gas.

For a segment of gas-liquid signal, in which the number of small discrete gas and liquid elements is N_a and N_w respectively, the probability of one element being gas ($\Pr(a)$) or liquid ($\Pr(w)$) is respectively:

$$\Pr(a) = \frac{N_a}{N_a + N_w} = C \quad (1)$$

$$\Pr(w) = \frac{N_w}{N_a + N_w} = 1 - C \quad (2)$$

where C is the time-averaged void fraction. Equations (1) and (2) assume implicitly no-slip between the gas and liquid interfaces, a quasi-steady streamtube velocity, and a significantly large number of gas-liquid elements, all of these being reasonable assumptions in high-velocity free-surface flows, e.g. as in Figure 1. The total number of gas-to-liquid interfaces equals that of liquid-to-gas interfaces. Considering the former, the average number of gas bubbles detected by the probe sensor per second equals the bubble frequency F :

$$F = N \Pr(a) \Pr(w) = \frac{U_{aw}}{\lambda_{aw}} C(1 - C) \quad (3)$$

where N is the average number of elemental interfaces detected by the probe sensor per second and U_{aw} the fluid velocity. Equation (3) predicts a quasi-parabolic relationship between bubble frequency and mean void fraction across the gas-liquid column, thus a pseudo linear relation between the root mean square of the instantaneous void fraction and the bubble frequency. An extended solution yields a relationship between bubble frequency and interfacial turbulence intensity (Zhang and Chanson 2016).

A few studies (Chanson and Gonzalez 2004, Gonzalez 2005) discussed the use of spectral analysis performed on the phase-detection probe signal output. The power spectral density (PSD) of a binary void fraction signal is defined as the square of the discrete Fourier transform (DFT) coefficients:

$$S_c = E \left(\text{FFT}(c') \text{FFT}^*(c') \right) \quad (4)$$

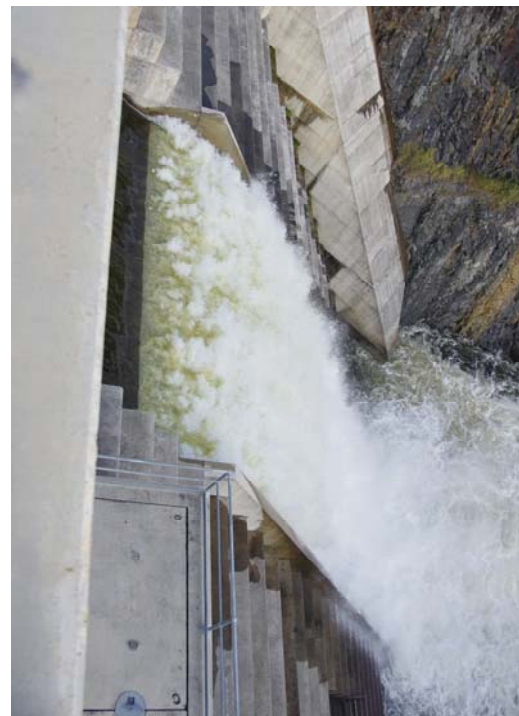
where S_c is the void fraction PSD, FFT is the fast Fourier transform, $*$ denotes the complex conjugate, c' is the instantaneous void fraction deviation from the mean value, and E is the expectation operator.

The shape of the void fraction PSD reflects contributions from all individual bubble/droplet sizes. The bandwidth of a bubble's contribution to the PSD is inversely proportional to its physical size. Namely, a small bubble/droplet contributes approximately equally to all frequencies, while a large

bubble/drop contributes predominantly to the low frequency range. A theoretical analysis shows that the void fraction power decays as $1/f^2$ at the end of the spectrum, where f is the frequency. Thus, a characteristic size of the smallest gas bubbles may be defined as $1/f_c$, where f_c is a characteristic frequency beyond which the PSD slope visually follows $1/f^2$.



(A) Laboratory experiment - $Q = 0.084 \text{ m}^3/\text{s}$, $Re = 3.4 \times 10^5$, $h = 0.10 \text{ m}$, $\theta = 45^\circ$



(B) Hinze dam prototype spillway on 7 May 2015 - $Q = 21 \text{ m}^3/\text{s}$, $Re = 6.7 \times 10^6$, $h = 1.2 \text{ m}$, $\theta = 51.3^\circ$

Fig. 1 Interfacial aeration along a stepped spillway chute

3. Void fraction spectra

The analysis of a single-sensor phase detection probe ($\varnothing = 0.25$ mm) was conducted in the stepped chute, and for the flow conditions, shown in Figure 1A. The water discharge was $Q = 0.071$ m³/s, the Reynolds number was $Re = 2.8 \times 10^5$, the vertical cavity height was $h = 0.10$ m, and the chute slope was $\theta = 45^\circ$. The phase-detection probe was sampled at 5 kHz for 180 s, as preliminary tests showed that a relatively long sampling duration was important as part of the proposed technique. Figure 3A shows the distributions of time-averaged void fraction and bubble frequency at step edge 12. The void fraction PSD was estimated using Welch's (1967) method. Each void fraction signal was first divided into 29 sub-segments, each of $1/15^{\text{th}}$ the total length of the signal, taken with a 50% overlap; each segment was then multiplied by a Hann window to reduce boundary effects before calculating discrete Fourier transform (DFT) was calculated. The final result was taken as the average over the 29 total modified PSDs. The void fraction signals were thresholded and detrended prior to computation. Figure 3B shows the void fraction spectrum data. In Figure 3B, let us note the variety of shapes displayed by the PSD curves at different elevations. By the Wiener-Khinchin theorem, $S_c(f)$ and $R_{xx,c}(\tau)$ form a Fourier transform pair. Therefore the area under each curve is proportional to the variance of the signal, equalling $C(1-C)$ (Murai et al. 2006). Thus, in the first approximation, the integral $\int S_c df$ is proportional to the bubble frequency F . More details are presented in the Appendix I.

The expected shape of a void fraction spectrum may be analysed theoretically by treating a binarised void fraction signal as a linear superposition of pulse trains, each characterised by a unique duration corresponding to the chord time of the bubbles under consideration. The expected shape of the void fraction spectra should follow:

$$E(S_c(f)) = \frac{1}{\pi^2 f^2 N} \left(\sum_{i=1}^{N_b} N_{bi} \sin^2(\pi f \tau_{ci}) + \frac{8}{\pi^2} \sum_{i=1}^{N_b-1} \sum_{j=i+1}^{N_b} N_i N_j \sin(\pi f \tau_{ci}) \sin(\pi f \tau_{cj}) \right) \quad (5)$$

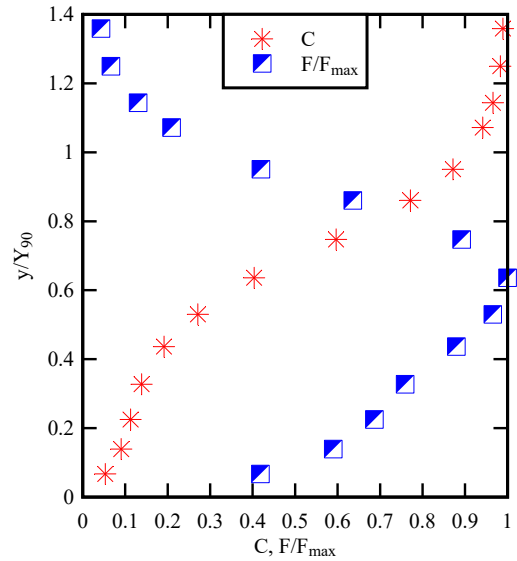
where N_b is the total number of bubbles in a pulse train, N_p is the total number of pulse trains, N is the total length of the signal, f is the frequency (horizontal axis of PSD data), and τ_c is a unique bubble chord time for each pulse train. The complete derivation is shown in Appendix I. Equation (5) holds for all $f \neq 0$, and the $S_c(0)$ term is simply zero if the data is detrended before calculation (i.e. zero mean). In Equation (5), the shape of a void fraction spectrum is the sum of contributions from each unique bubble chord time as well as interactions between every pair of chord times. A detailed interpretation of the properties of Equation (5) is developed in Appendix I.

In summary, the dependence of $E(S_c(f))$ on a single chord time τ_{ci} reflects the fact that a narrow (wide) band signal in the frequency domain have a wide (narrow) counterpart in the time domain, namely:

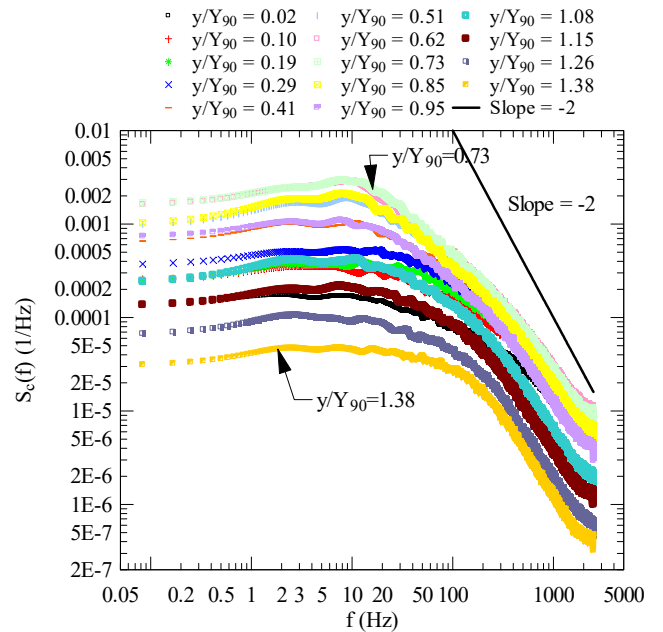
(a) for $\tau_{ci} \approx 0$ (very small bubbles/droplets), the contribution is approximately equal to all frequency components in the PSD; and

(b) for $\tau_{ci} \gg 0$ (very large bubbles/droplets), the contribution is dominantly to the low frequency range in the PSD and decays with $1/f^2$ in the high frequency range;

Consequently, the high frequency range of the PSD curve reflects contributions of small chord times, whereas the low frequency range contains contributions of both small and large chord times. Likewise, the interactions between the smallest bubbles contribute approximately uniformly to the entire frequency range of the spectrum, while any interaction involving large bubbles/droplets will be modulated by $1/f^2$.



(A) Vertical distributions of time-averaged void fraction C and bubble frequency F



(B) Void fraction spectra in the stepped chute flow

Fig. 3 Void fraction distribution and spectra in a stepped chute flow - $Q = 0.084 \text{ m}^3/\text{s}$, $Re = 3.4 \times 10^5$, $h = 0.10 \text{ m}$, $\theta = 45^\circ$, step edge 12, $Y_{90} = 0.0518 \text{ m}$, $V_{90} = 4.10 \text{ m/s}$, $F_{\max} = 272 \text{ Hz}$

3.1. Discussion

Gonzalez (2005) hinted that the void fraction spectrum may be divided into two zones about a characteristic frequency f_c : i.e. $f < f_c$ and $f > f_c$, each representing the total energy in the signal due to the largest and smallest length scales, where f_c may be identified from a change in slope in the spectra. In the present study, Equation (5) suggests that both small and large length scales contributed to the low frequency range of the spectrum. Rather, a characteristic frequency f_c may be defined as where the spectrum visually follows $1/f^2$. In such case, U_{aw}/f_c could be loosely interpreted as the smallest air bubble length scale in the flow.

In reference to Figure 3B, a preponderance of small chord times is observed next to the step edge (red and black curves) and large chord times are dominant in the spray zone ($y/Y_{90} > 1$). The former case reflects the large rate-of-strain next to the step edge, where a significant number of small bubbles are generated. The latter case implies a flow primarily consisting of water globules of large chord sizes.

4. Conclusion and future work

The present study indicates that the void fraction PSD may be used to provide an alternative view of the air-water flow composition, including a new way to interpret the information contained in the PSD of a phase function signal. Information such as the bubble count rate and characteristic air-water chord size can be inferred. The void fraction distribution is implied by combining the bubble count rate and air-water chord size information: e.g. small bubble count rate and large chord size imply low void fraction.

The dependence of the void fraction spectrum $E(S_i(f))$ on a single chord time τ_{ci} reflects the fact that a narrow (wide) band signal in the frequency domain have a wide (narrow) counterpart in the time domain. The high frequency range of the PSD curve reflects contributions of small chord times, while the low frequency range contains contributions of both small and large chord times. Likewise, the interactions between the smallest bubbles contribute approximately uniformly to the entire frequency range of the spectrum, while any interaction involving large bubbles/drops will be modulated by $1/f^2$. Importantly, the void fraction spectra are a powerful tool in providing an alternative view of the air-water flow composition. This method has the advantage of aggregating a number of qualitative information in one glance, including the bubble count rate and air-water chord sizes. The void fraction might be inferred by combining the bubble count rate and air-water chord size information (e.g. small bubble count rate and large chord size imply low void fraction).

5. Acknowledgments

The authors acknowledge the financial supports of the Australian Research Council (Grant DP120100481), and the technical assistance of Jason Van Der Gevel and Matthews Stewart (The University of Queensland).

6. Appendix I - Spectral properties of a binary void fraction signal (Supplementary material)

See Supplementary material.

References

- Bertola, N.J., Wang, H., and Chanson, H. (2018), "Air Bubble Entrainment, Breakup and Interplay in Vertical Plunging Jets." *Journal of Fluids Engineering*, ASME, Vol. 140, No. 9, Paper 091301, 13 pages (DOI: 10.1115/1.4039715).
- Cain, P., and Wood, I.R. (1981). "Measurements of Self-aerated Flow on a Spillway." *Jl. Hyd. Div.*, ASCE, 107, HY11, pp. 1425-1444.
- Cartellier, A., and Achard, J.L. (1991). "Local Phase Detection Probes in Fluid/Fluid Two-Phase Flows." *Rev. Sci. Instrum.*, Vol. 62, No. 2, pp. 279-303.
- Chanson, H. (1997). "Air Bubble Entrainment in Free-Surface Turbulent Shear Flows." *Academic Press*, London, UK, 401 pages.
- Chanson, H. (2002). "Air-Water Flow Measurements with Intrusive Phase-Detection Probes. Can we Improve their Interpretation?" *Journal of Hydraulic Engineering*, ASCE, Vol. 128, No. 3, pp. 252-255 (DOI: 10.1061/(ASCE)0733-9429(2002)128:3(252)).
- Chanson, H. (2016). "Phase-Detection Measurements in Free-Surface Turbulent Shear Flows." *Journal of Geophysics and Engineering*, Vol. 13, No. 2, pp. S74-S87 (DOI: 10.1088/1742-2132/13/2/S74).
- Chanson, H., and Gonzalez, C.A. (2004). "Interactions between Free-surface, Free-stream Turbulence and Cavity Recirculation in Open Channel Flows: Measurements and Turbulence Manipulation." *Proceedings 5th International Conference on Multiphase Flow*, Yokohama, Japan, Y. Matsumoto, K. Hishida, A. Tomiyama, K. Mishima and S. Hosokawa editors, Paper 104, 14 pages.
- Crowe, C., Sommerfeld, M., and Tsuji, Y. (1998). "Multiphase Flows with Droplets and Particles." *CRC Press*, Boca Raton, USA, 471 pages.
- Ervine, D.A., McKeogh, E.J., and Elsayy, E.M. (1980). "Effect of Turbulence Intensity on the rate of Air Entrainment by Plunging Water Jets." *Proc. Instn Civ. Engrs*, Part 2, June, pp. 425-445.
- Felder, S., and Chanson, H. (2016). "Air-water flow characteristics in high-velocity free-surface flows with 50% void fraction." *International Journal of Multiphase Flow*, Vol. 85, pp. 186-195 (DOI: 10.1016/j.ijmultiphaseflow.2016.06.004).
- Gnedenko, B.V., and Kolmogorov, A.N. (1949). "Limiting distributions for sums of independent random quantities." *Gostekhizdat*, Moscow.
- Gonzalez, C.A. (2005). "An Experimental Study of Free-Surface Aeration on Embankment Stepped Chutes." *Ph.D. thesis*, Department of Civil Engineering, The University of Queensland, Brisbane, Australia.
- Hoyt, J.W., and Taylor, J.J. (1977). "Turbulence Structure in a Water Jet Discharging in Air." *Physics of Fluids*, Vol. 20, No. 10, Pt. II, Oct., pp. S253-S257.
- Jones, O.C., and Delhay, J.M. (1976). "Transient and Statistical Measurement Techniques for two-Phase Flows: a Critical Review." *International Journal of Multiphase Flow*, Vol. 3, pp. 89-116.
- Mirai, Y., Oishi, Y., Takeda, Y., and Yamamoto, F. (2006). "Turbulent Shear Stress Profiles in a Bubbly Channel Flow Assessed by Particle Tracking Velocimetry." *Experiments in Fluids*, Vol. 41, pp. 343-352.
- Oppenheim, A.V., and Schaffer, R.W. (2010). "Discrete-time signal processing." *Pearson*, Upper Saddle River N.J., 3rd edition, 1108 pages.
- Papoulis, A., and Pillai, S.U. (2002). "Probability, random variables, and stochastic processes." *McGraw-Hill*, Boston, 4th edition, 852 pages.

Press, W.H., Flannery, B.P., Teukolsky, S.A., and Vetterling, W.T. (1986). "Numerical recipes: the art of scientific computation." *Cambridge University Press*, Cambridge Cambridgeshire; New York, 818 pages.

Rao, N.S.L., and Kobus, H.E. (1971). "Characteristics of Self-Aerated Free-Surface Flows." *Water and Waste Water/Current Research and Practice*, Vol. 10, Eric Schmidt Verlag, Berlin, Germany.

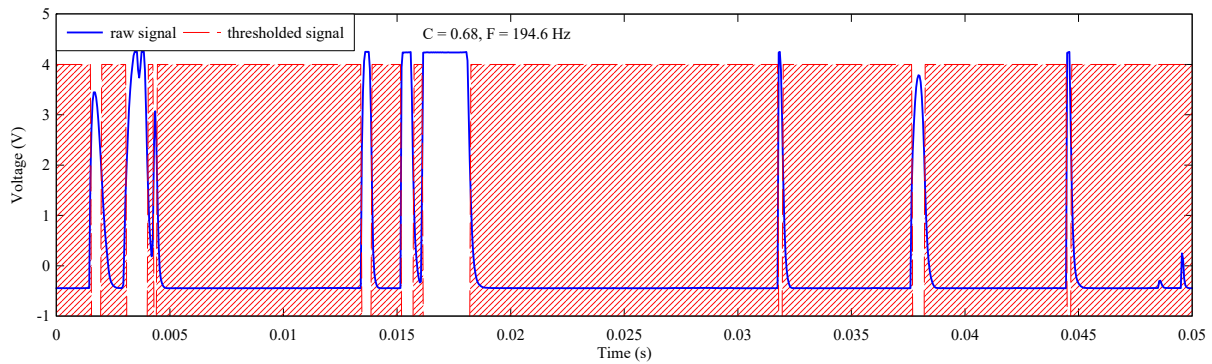
Toombes, L., and Chanson, H. (2008). "Interfacial Aeration and Bubble Count Rate Distributions in a Supercritical Flow Past a Backward-Facing Step." *International Journal of Multiphase Flow*, Vol. 34, No. 5, pp. 427-436 (doi.org/10.1016/j.ijmultiphaseflow.2008.01.005).

Welch, P. (1967). "The use of fast fourier transform for the estimation of power spectra: A method based on time averaging over short, modified periodograms." *IEEE Transactions on Audio and Electroacoustics*, Vol. 15, No. 2, pp. 70-73. (DOI:10.1109/TAU.1967.1161901).

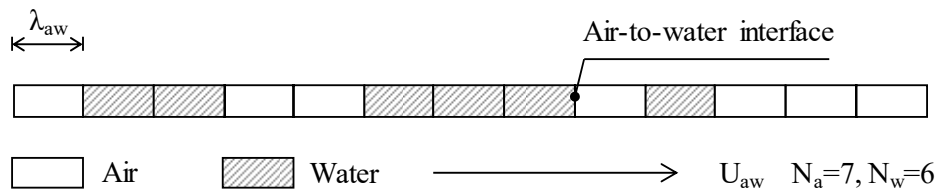
Wood, I.R. (1991). "Air Entrainment in Free-Surface Flows." *IAHR Hydraulic Structures Design Manual No. 4*, Hydraulic Design Considerations, Balkema Publ., Rotterdam, The Netherlands, 149 pages.

Zhang, G., and Chanson, H. (2016). "Interactions between Free-surface Aeration and Total Pressure on a Stepped Chute." *Experimental Thermal and Fluid Science*, Vol. 74, pp. 368-381 (DOI: 10.1016/j.expthermflusci.2015.12.011)

Zhang, G., and Chanson, H. (2017). "Self-aeration in the rapidly- and gradually-varying flow regions of steep smooth and stepped spillways." *Environmental Fluid Mechanics*, Vol. 17, No. 1, pp. 27-46 (DOI: 10.1007/s10652-015-9442-z).



(A) Phase-detection probe signal output in a stepped chute - $Q = 0.084 \text{ m}^3/\text{s}$, $Re = 3.4 \times 10^5$, $h = 0.10 \text{ m}$, $\theta = 45^\circ$, mean void fraction: $C = 0.68$



(B) Streamwise distribution of discrete two-phase elements assuming $\lambda_{aw} = \lambda_a = \lambda_w T$, following Toombes and Chanson (2008)

Fig. 2 Gas-liquid flow structure detected by a phase-detection needle probe